Andean Geology 53 (1): 98-112. January, 2025
doi: 10.5027/andgeoV53n1-3768

Andean Geology
www.andeangeology.cl

Using Ground Penetrating Radar (GPR) to identify sediment morphology and buried large wood in volcanic deposits, Blanco River, southern Chile

***Galo Valdebenito[1, 2], Andrés Iroumé[2, 3], David Alvarado[2], Carlos Fuentes[2], Lorenzo Picco[1, 2, 4]**

[1] *Universidad Austral de Chile, Facultad de Ciencias de la Ingeniería, General Lagos 2086, Valdivia, Chile.*
gvaldebe@uach.cl, lorenzo.picco@unipd.it

[2] *RiNA Núcleo de Investigación en Riesgos Naturales y Antropogénicos, Universidad Austral de Chile, Ganeral Lagos 2086, Valdivia, Chile.*
airoume@uach.cl, david.alvarado@uach.cl, krlo.ffi@hotmail.com

[3] *Universidad Austral de Chile, Facultad de Ciencias Forestales y Recursos Naturales, Avda. Zoltan Nagy Yanstsky s/n, Campus Isla Teja, Valdivia, Chile.*

[4] *Università degli Studi di Padova, Dipartimento Territorio e Sistemi Agro Forestali, Viale dell'Università 16, 35020, Legnaro (PD), Italia.*

***** *Corresponding author: gvaldebe@uach.cl*

ABSTRACT. Snow avalanches, landslides, and debris flows are the primary mechanisms delivering wood to streams in steep, forested headwater catchments. Tree mortality and bank erosion, in contrast, play a relatively major role in recruiting large wood (LW) in larger watersheds. The 2008-2009 explosive eruption of the Chaitén volcano in southern Chile caused widespread forest destruction, depositing several meters of volcanic sediments and dead wood in the Blanco River valley. Tephra fall, pyroclastic density currents, and dome collapses filled the valley, creating thick deposits of lithic-rich gravelly sand and buried wood. Post-eruption fluvial processes and channel adjustments have since eroded these deposits, mobilizing buried dead wood into the channel and creating an additional, previously understudied LW recruitment process. The exhumation of buried wood pieces could increase downstream risks during floods, emphasizing the importance of understanding this process. Given that buried wood cannot be visually identified, the prospecting non-invasive geophysics technique based on Ground Penetrating Radar (GPR) was used in this study to perform continuous scanning of the lithic-rich volcanic deposits along the Blanco River. Three key research questions were addressed: 1) Can the internal morphology and structure of volcanic deposits be described using GPR?; 2) Can GPR detect the signature of buried wood within these deposits?; and 3) Is it possible to determine the spatial distribution of buried LW using high-resolution 3D subsurface mapping of GPR reflections? Following initial calibration, GPR scanning produced radargram profiles that were post-processed into 2D and 3D representations of the deposits, successfully identifying buried LW, whose spatial distribution was subsequently mapped using 3D GPR analysis. This study demonstrates that GPR is a rapid, non-invasive, and precise tool for characterizing the morphology and internal structure of river sediments affected by volcanic activity, facilitating the identification of buried LW.

Keywords: Ground Penetrating Radar, Buried wood, Depositional fluvial morphology, Pyroclastic deposits, Chaitén Volcano, Chile.

RESUMEN. Uso de Radar de Penetración Terrestre (GPR) para identificar la morfología de los sedimentos y la madera de gran tamaño enterrada en depósitos volcánicos, río Blanco, sur de Chile. Las avalanchas de nieve, los deslizamientos de tierra y los flujos de detritos son los principales mecanismos que aportan madera de gran tamaño (LW, por sus siglas en inglés) a los cursos de agua en cabeceras de cuencas boscosas y de fuerte pendiente. En contraste, la mortalidad de árboles y la erosión de riberas desempeñan un papel relativamente mayor en el reclutamiento de LW en cuencas de mayor tamaño. La erupción explosiva del volcán Chaitén (2008-2009), en el sur de Chile, provocó una destrucción generalizada del bosque, depositando varios metros de sedimentos volcánicos y madera muerta en el valle del río Blanco. Este valle fue rellenado por depósitos de caída de tefra, corrientes de densidad piroclástica y colapsos parciales del domo volcánico, generando secuencias de gravas y arenas de gran espesor ricas en litoclastos y madera

enterrada. Los procesos fluviales y los ajustes del cauce han, desde entonces, erosionado estos depósitos, movilizando la madera muerta enterrada hacia el cauce y generando un proceso adicional de reclutamiento de LW, hasta ahora poco estudiado. La exhumación de piezas de madera enterrada podría aumentar los riesgos aguas abajo durante crecidas, lo que resalta la importancia de comprender este proceso. Dado que la madera enterrada no puede ser identificada visualmente, se utilizó en este estudio la técnica geofísica no invasiva de prospección basada en radar de penetración terrestre (GPR, por sus siglas en inglés), para realizar un escaneo continuo de los depósitos volcánicos ricos en litoclastos a lo largo del río Blanco. Se abordaron tres preguntas de investigación: 1) ¿Es posible describir la morfología y la estructura interna de los depósitos volcánicos mediante GPR?; 2) ¿Puede el GPR detectar la señal de la madera enterrada en estos depósitos?; y 3) ¿Es posible determinar la distribución espacial de la LW enterrada mediante un mapeo subsuperficial tridimensional de alta resolución a partir de reflexiones GPR? Tras una calibración inicial, el escaneo GPR produjo perfiles de radargramas que fueron procesados en representaciones 2D y 3D de los depósitos, identificando con éxito la LW enterrada, cuya distribución espacial fue posteriormente mapeada mediante análisis 3D de GPR. Este estudio demuestra que el GPR es una herramienta rápida, no invasiva y precisa para caracterizar la morfología y la estructura interna de sedimentos fluviales afectados por actividad volcánica, facilitando la identificación de la LW enterrada.

Palabras clave: Radar de penetración terrestre, Madera enterrada, Morfología fluvial depositacional, Depósitos piroclásticos, Volcán Chaitén, Chile.

1. Introduction

In steep forested headwater catchments, snow avalanches, landslides, and debris flows typically dominate large wood (LW, wood pieces ≥1 m long and ≥10 cm in diameter; Iroumé *et al.*, 2015) delivery to streams. In larger watersheds, however, tree mortality and bank erosion are more important in recruiting LW into the active channel (Martin and Benda, 2001; May and Gresswell, 2003; Reeves *et al.*, 2003; Picco *et al.*, 2016). In each reach, the LW budget is a consequence of the balance between the amount of wood stored and recruited, and the ability of the stream to transport logs through the active channel and from upstream to downstream reaches (Martin and Benda, 2001; Benda and Bigelow, 2014; Schenk *et al.*, 2014). Wood decay and breakage (Iroumé *et al.*, 2017) are additional components to wood budgeting, especially when mass balances are performed for long time periods (Wohl, 2013).

Wohl (2017) highlighted the challenges of LW budgeting, particularly because some of its components are difficult to analyse. More recently, and depending on the timescale, interdecadal and interannual budgets and load fluctuations have been proposed from various riverine environments (Boivin *et al.*, 2017; Tonon *et al.*, 2018; Iroumé *et al.*, 2020a; Picco *et al.*, 2021). However, much work remains to be done, especially in addressing the influence of large infrequent disturbances (LIDs; Foster *et al.*, 1998) on LW budgeting. Among these, explosive volcanic eruptions have the capacity to rapidly kill and obliterate island and riparian forests, and to fill river valleys with excess pyroclastic material and large wood, generating deposits several meters thick (*e.g.*, Pierson and Major, 2014; Tonon *et al.*, 2017), increasing dramatically the dynamicity of sediments and wood, and favoring continuous morphological changes. This is the case of the Blanco River (southern Chile) that was severely affected by the 2008-2009 Chaitén volcanic eruption (Major *et al.*, 2013, 2016; Pierson *et al.*, 2013; Swanson *et al.*, 2013; Ulloa *et al.*, 2015; Iroumé *et al.*, 2020b). In this river, lateral migrations of the main channel still expose and incorporate huge amounts of buried LW stored into the volcanic deposits all over the valley floor of the river basin (Fig. 1).

Although Martin and Benda (2001) included exhumation of buried wood as a recruitment process in their wood budgeting proposal, the external visual identification of buried LW is not possible; then, increasing the detection of buried wood will consequently improve wood budgeting analyses. On the other hand, characterization of the morphology and stratigraphy of fluvial sedimentary deposits in volcanic environments, is an important task that normally helps in the understanding of the volcanic processes and the relationships with sediment transport and buried LW recruitment (Jara, 2015; Fuentes, 2016; Barrientos, 2020). In this sense, the study of the internal morphology and structure of volcano-sedimentary deposits (*e.g.*, Gomez *et al.*, 2008) notably improves the identification and characterization of buried LW.

Traditional methods for identifying buried wood involve digging, trenches, excavations, and similar interventions that allow for direct observation. These invasive approaches can be time- and resource-

FIG. 1. Buried LW (~3 m-long) exposed by lateral migration of the Blanco River channel (photo from upstream to downstream, by A. Iroumé).

intensive, requiring significant labor or machinery, which may be challenging to transport to specific study sites. Therefore, electromagnetic non-invasive geophysical surveys using Ground Penetrating Radar (GPR) have emerged as a possible solution to study the internal morphology and stratigraphy of volcanic deposits (Cassidy *et al.*, 2003; Burke *et al.*, 2008, 2010; Hornung *et al.*, 2010; Ashworth *et al.*, 2011; Kramer *et al.*, 2012; Rey *et al.*, 2013). In volcanic sedimentology, GPR has been extensively used to determine the thickness of the deposits (Jinder *et al.*, 2006; Gómez *et al.*, 2008; Gertisser *et al.*, 2012). Moreover, different studies aimed at detecting root patterns and the biomass of living trees are using GPR as a rapid and non-invasive technique compared with traditional methods (Butnor *et al.*, 2001; Gómez *et al.*, 2008; Satriani *et al.*, 2010; Gertisser *et al.*, 2012; Borden *et al.*, 2014; Butnor *et al.*, 2016; Liu *et al.*, 2018).

To improve the use of GPR, it is relevant to combine different methods to post-process the data obtained in the field. Normally, conventional post-processing consists of a static correction, a displacement correction, noise reduction in one and two dimensions, and gain adjusts (Jara, 2015; Fuentes, 2016; Barrientos, 2020). In addition, root detection studies have also successfully incorporated a migration method and Hilbert transform as a part of their processing chain, achieving more detailed and clearer results (Guo *et al.*, 2013). The purpose of static correction is to adjust the zero time of each trace to account for early recordings of air and direct waves, ensuring accurate depth measurements (Yelf and Yelf, 2004). Two-dimensional filtering removes common noise in traces, typically from direct and aerial waves, the radar itself, or other sources (Jara, 2015). In addition, electromagnetic signals weaken over time due to attenuation from absorption, dispersion, and spherical divergence, leading to information loss (*e.g.*, Neto and De Medeiros, 2006). To counteract this, a gain function amplifies wave amplitudes, especially for signals farther from zero time (Neto and De Medeiros, 2006); although excessive gain can introduce noise, reducing image quality. Consistent wave amplitude

across traces is crucial for analyzing deeper sediment layers. While hyperbolic reflections often identify pipes or objects (Jara, 2015), additional information on depth, size, and electromagnetic (EM) reflectivity is sometimes essential. Migration algorithms convert hyperbolic reflections into focused points, enhancing object localization and scattering amplitude (Özdemir *et al.*, 2014).

However, to date, GPR has not been used to explore the presence and spatial distribution of LW buried in pyroclastic deposits. Focused on this, the aim of this study is to assess the potential of using geophysical surveys based on GPR techniques to characterize the shallow stratigraphy of volcanic deposits and identify the signature of the buried LW. The latter step is crucial, as LW exhumation can heighten downstream risks associated with wood transport during floods.

2. Materials and methods

2.1. Study area

The present study was carried out along the Blanco River, severely affected by the 2008-2009 explosive eruption of the Chaitén volcano (Fig. 2). Detailed information on this eruption and the sedimentologic processes along the Blanco River basin can be found in Major and Lara (2013), Major *et al.* (2013, 2016), Pierson *et al.* (2013), Swanson *et al.* (2013), Ulloa *et al.* (2015), and Martini *et al.* (2019), among others.

The study site is located within the right bank of the lower course of the Blanco River, around 0.5 km upstream the village of Chaitén (Fig. 3A). The GPR field surveys were performed in a control area of volcano-sedimentary deposits (Fig. 3B, C). These deposits were classified as "very poorly sorted, unstratified, lithic-rich gravelly sand" by Major *et al.* (2013).

3. Ground Penetrating Radar

Ground Penetrating Radar (GPR) is a geophysical technique based on the detection of reflections generated from the emission of an electromagnetic pulse, which propagates through a discontinuous medium. Reflections and diffractions of electromagnetic waves occur at the boundaries between two different mediums that have different electrical properties, which happens due to either different soil layers or the presence of singularities within the medium. The physical parameters that determine the reflectivity of the layer boundaries and the penetration depth are the electric permittivity ε and the electrical conductivity σ (Knödel *et al.*, 2007).

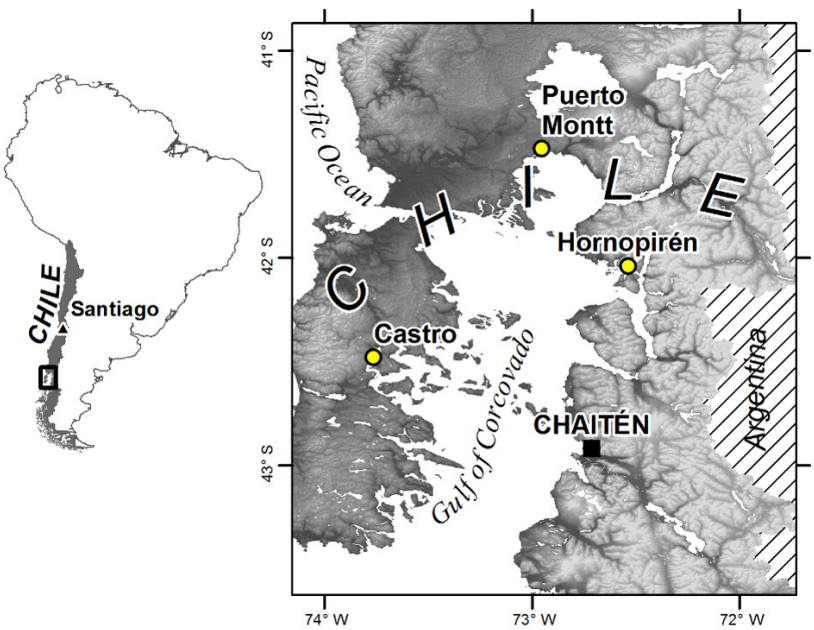

FIG. 2. Location of Chaitén volcano in southern Chile (black square). Relevant towns are shown as yellow circles.

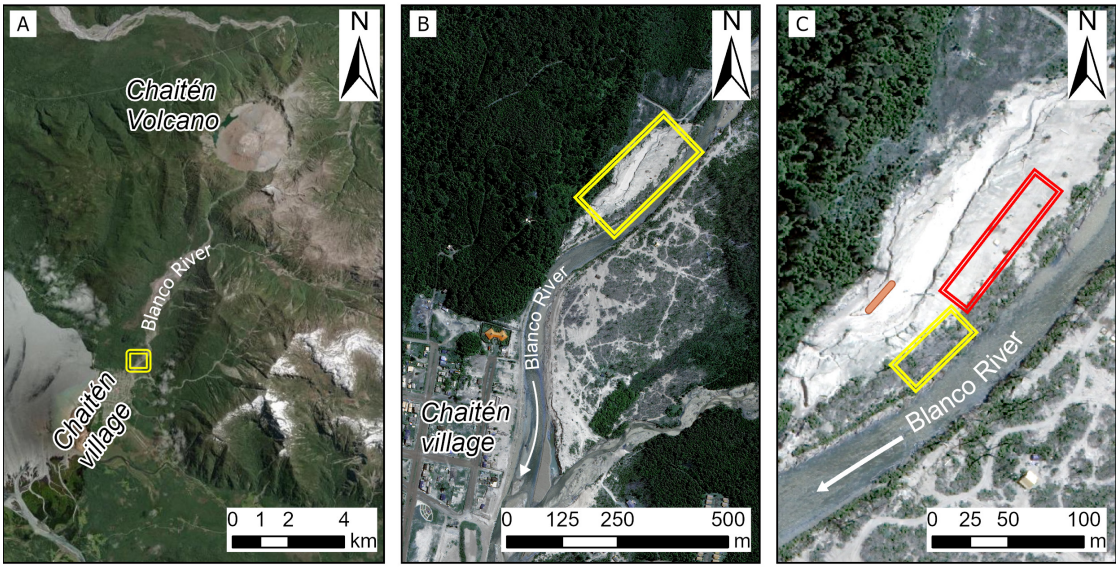

FIG. 3. Village of Chaitén, the Blanco River, and Chaitén volcano locations. **A.** Study site (yellow rectangle) along the lower course of the Blanco River. **B.** Zoom location of the study site (yellow rectangle), with respect to the village of Chaitén. **C.** Details of the surveyed zone where calibration (solid orange line) and field explorations (red and yellow rectangles) were carried out. Satellite images from Google Earth.

The propagation velocity (v) of the electromagnetic wave is related to the dielectric constant (εr) of each material (Eq. 1).

$$\sqrt{\varepsilon_r} = \frac{c}{v}$$

Where c is the propagation velocity of the electromagnetic wave in the air (c=3×108 m s-1). This relationship, combined with the reflected wave travel time, forms the basis for locating detected singularities, with proper post-processing ensuring successful interpretation.

Basically, the equipment in the field is composed of a control unit, the antenna (wave generation and reception), and a computer to visualize and collect the data. As the equipment moves forward on the surveyed surface, the transmitting antenna generates electromagnetic wave pulses, while the receiving antenna measures the reflected wave amplitude of each pulse as a function of time, generating a continuous image of the travel times of the reflected waves. When the traces are plotted as a function of distance, a bi-dimensional continuous representation of the subsoil is obtained, called a radargram. Because the technique implies continuous motion of the antenna, the field survey is simple and fast in comparison with more classical static geophysical electromagnetic strategies. The adequate selection of the antenna is vital because the resolution and penetration capability depend, among other things, on the central frequency of the antenna. In this sense, low frequency antennas (typically lower than 250 MHz) have higher penetration capability but limited superficial resolution (Utsi, 2014). In addition, being an electromagnetic method, the resolution and penetration capacity in the medium depend on the magnetic permeability and electrical conductivity of the material (Baker *et al.*, 2007). For this study, an analog monochannel MALÅ® RAMAC X3M GPR unit considering 250 and 500 MHz shielded antennas was used.

4. Field calibrations and channel surveys

The GPR surveys were divided into two phases: 1) calibration surveys to define the more adequate antennas, field parameters (velocities, stacking, field filtering) and the search for the signature of buried LW; and 2) field data acquisition following the lines of a control grid for both 2D and 3D subsurface explorations.

The calibration surveys were carried out in the location of a gully developed in the volcanic

deposits (Fig. 3C). This location provided access to characterize the deposit layering and stratigraphic characteristics in detail. Odometer calibration, adjust of the stacking (frequency of the electromagnetic pulses) and field filtering were first performed in the control area. Secondly, metallic bars and wood pieces with different and known diameters were inserted horizontally at specific depths into the almost vertical profile of the deposit along the right bank of the gully (Fig. 4A, B). This procedure allowed the definition of the more adequate GPR antennas, and to capture the shape and geometry of the hyperbolic reflections (here called signature) in the radargrams associated with these artificially inserted specimens (Fig. 4C). In this calibration, both shielded antennas (250 and 500 MHz) were used to select the more appropriate in the channel surveys. Finally, by adjusting in the post-processed radargrams the reflection of the metal bars to their real, measured depths, it was possible to determine a speed of propagation of the wave in the medium of 90±5 m/μs for wet ash. This parameter allowed to estimate the depths of the objects found and to determine the maximum exploration depths in the medium.

From the high resolution radargrams generated with the antennas, hyperbolas associated with reflections of LW could be identified. The 250 MHz antenna generated radargrams with a maximum penetration depth of 8 m, while those derived using the 500 MHz antenna only penetrated up to 5 m. According to this, the field data acquisition following the lines of the control grid for both 2D and 3D explorations were completed using the GPR with both antennas.

To interpret the signature of buried LW, both LW pieces and metallic bars were introduced into the deposits to differentiate them in the post-processed radargrams (red circles in figure 5). With this procedure, it was easier to identify the desired targets (LW) and their signatures. In addition, it

FIG. 4. **A.** GPR operating along the edge of the gully, woody logs were installed into the steep bank of the gully as control objects (circles). **B.** Field photograph of the gully where the measures were carried out (about 3.6 m-high). **C.** Radargram obtained from profile shown on A.

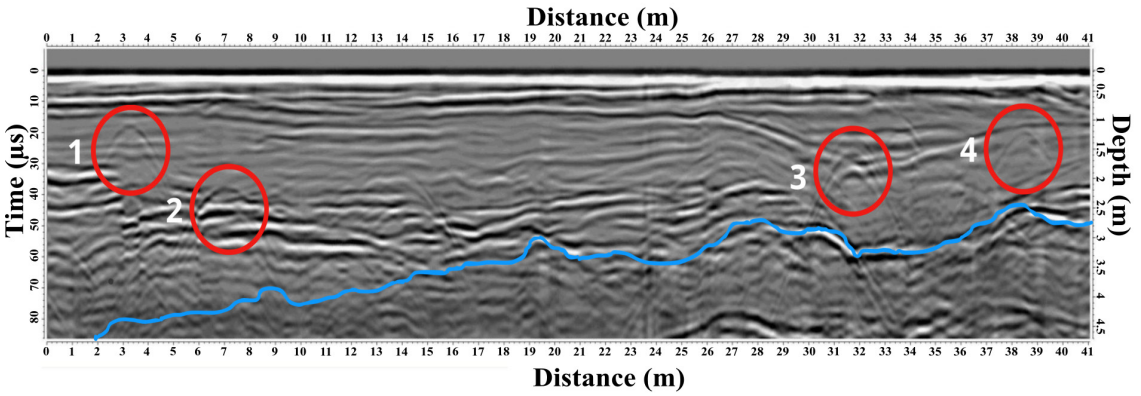

FIG. 5. Identification of the different elements according to table 1. Red, numbered circles enclose the singularities identified. The blue line shows the base level associated with the pre-eruptive surface.

was possible to identify the deep contrast (blue line in figure 5) associated with the reflections of the base level. Table 1 reports the main properties of the specimens related to the singularities identified in figure 5.

TABLE 1. ARTIFICIAL SPECIMENS INTRODUCED FOR SIGNATURE CHARACTERIZATION.

Element	Detail	Diameter (cm)	Depth (m)
1	LW	50	0.75
2	Metallic bar	4	2
3	LW	6	1.05
4	LW (in group)	25	1.15

To generate 3D mappings, evenly spaced profile lines were used to define a grid in the field, which allowed the generation of multiple 2D radargrams. Common points acting as constraints were identified and combined to correlate each 2D mapping and create a 3D view. The grid layouts were selected as a starting point based on traditional surveys using geophysical methods in the identification of underground pipelines.

To compare data quality and resolution, two grids were tested: 1) South grid, 100x20 m rectangle with surveys each 5 m using the 250 MHz antenna; 2) North grid, 20x18 m rectangle with surveys each 3 m using 500 and 250 MHz antennas. Both grids were georeferenced with a double-frequency GPS Trimble® R5 PP/RTK (3 and 3.5 mm of horizontal and vertical precision, respectively) to correctly define each profile. The GPR with the 250 MHz antenna was carried along each of the previously defined lines of the grid. In this sense, figure 6 explains with two orthogonal radargrams this procedure. In this figure obtained from the grid, the bed rock (black line) is visible in which the depths are compatible for both images.

5. Post-processing of radargrams

Radargrams were post-processed to clean and adjust for rare and disordered contaminated reflections. Post-processing combined conventional static correction, displacement correction, noise reduction in one and two dimensions, and gain adjusts (Jara, 2015), as well as a migration method and Hilbert transform. Low frequency noises can sometimes generate a phase shift in the amplitude domain of each trace; these can be corrected by applying a 1D band-pass Butterworth filter, with a lower cut-off value equal to half the central frequency and an upper cut-off value equal to one and a half times the central frequency of the shielded antenna (Baker *et al.*, 2007).

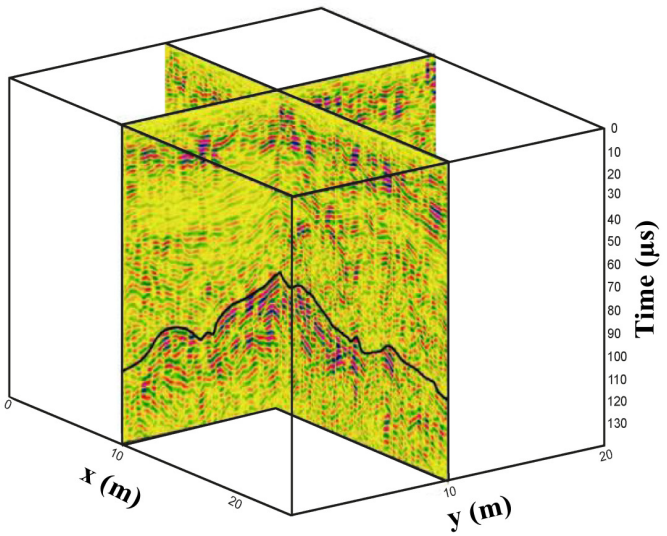

FIG. 6. Representation of two perpendicular 2D radargrams to facilitate a 3D analysis of the subsoil below the study grid.

When it comes to migration methods, one of the most commonly applied in GPR post-processing is the Kirchhoff migration, which requires estimating the EM wave velocity (Guo *et al.*, 2013). Another advanced post-processing technique, which complements the above mentioned, is the Hilbert transform, a mathematical tool that expresses the relationship between the magnitude and the phase of the radar signal (Oppenheim and Schafer, 2014). It can also be described as an "envelope of amplitudes", that takes positive and negative values from a recorded trace and extracts the pulse envelope that measures the signal power. The magnitude part of the Hilbert transform indicates the pattern of absorbance of the incident energy of the GPR whereas the phase component indicates how the incident energy is filtered in the subsurface (Pujari *et al.*, 2007). By applying this tool after the conventional post-processing and migration steps, the energetic content of different reflections can be compared. As the Hilbert transform converts the singularities observed in radargrams into focused points that represent the concentrated energy associated with specific reflections, this approach was used in the present study to investigate the potential detection and dimensions of buried LW. In this sense, this procedure is sought to be a first step for the diameter characterization of potentially buried LW by means of GPR technique. Finally, to improve the results according to the targets defined, GPR data were post-processed with REFLEXW (Sandmeier, 2009).

6. Results

6.1. 2D modelling: stratigraphy of volcanic deposits

The radargrams analyzed show the interface between the pre-eruptive surface and the 2008-2009 volcanic deposits (Fig. 7A). The depth of the base is in the range 3.5-4 m, which is consistent with

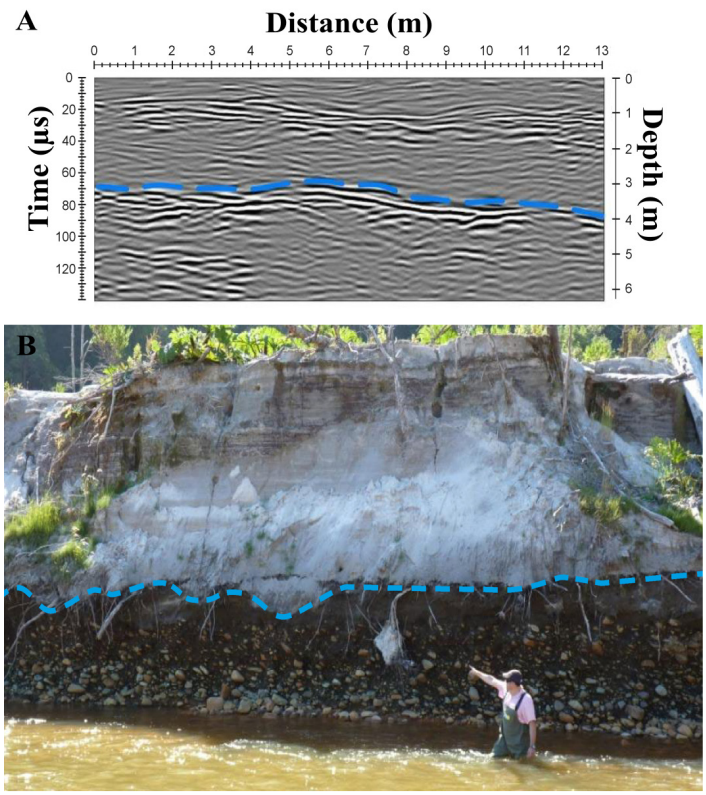

FIG. 7. **A.** Post-processed radargram obtained with the 250 MHz antenna in the surveyed site. The blue dashed line marks the reflection due to changes in the stratigraphy, indicating the pre-eruptive surface. **B.** Field evidence in a nearby site showing the contrast between the 2008-2009 volcanic deposits and the pre-eruptive surface, fitting with the obtained, post-processed radargrams.

the field observations done near the Blanco River (Fig. 7B). Figure 8 shows a radargram post-processed with the Hilbert transform, which increases the contrast and resolution of the volcanic deposits related to the pre-eruption level base.

6.2. 2D modelling: Identification of buried LW

Through the hyperbolic adjustment of media velocities, very similar values were found, indicating depth values that match the depths of the studied deposits. We also obtained good-resolution hyperbolic reflections generated by the pieces of LW embedded in the deposits (Fig. 9). The location and depth of the reflections coincided with the *ad hoc* buried wood pieces, allowing the definition of the LW signature for pieces of different sizes. These signatures are geometrically similar with respect to those identified with the control objects (Fig. 4C).

During post-processing, the application of the Kirchhoff migration and the Hilbert transform allowed a more precise determination of the location of buried LW and an initial estimation of the size (diameter) of each wood piece (Fig. 10).

6.3. 3D Modelling: Spatial variability of LW

The spatial variability of the buried LW was identified through 3D modelling, with their singularities recognized in sequences of radargrams. Due to the minor distance between profiles, results were more detailed in the north grid. Figure 11 shows a 3D model of the north grid identifying the location of buried LW. In this case, the length of each singularity and

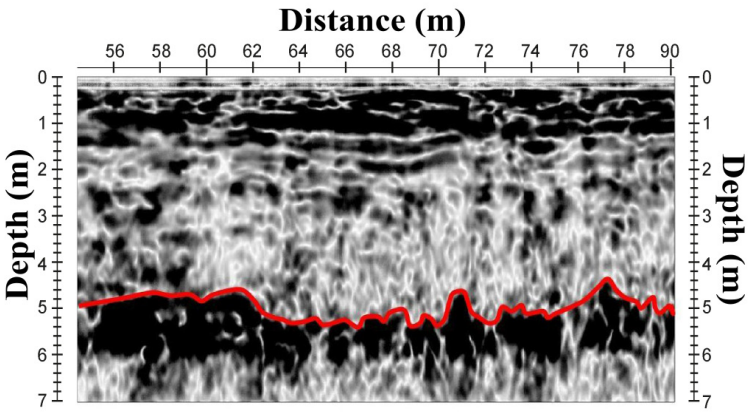

FIG. 8. Pre-eruptive surface (red line). Identified after applying Hilbert transform post-processing techniques.

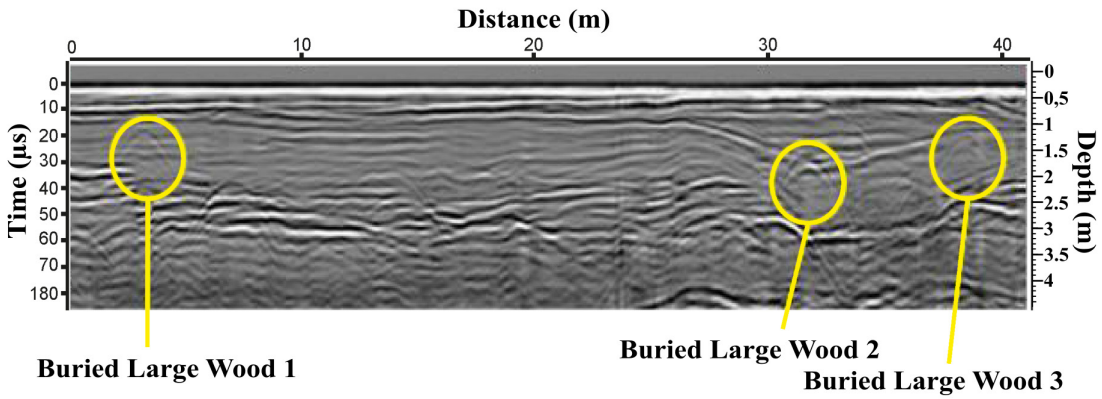

FIG. 9. Radargrams showing typical reflections due to LW present in the grids. Three LW specimens can be identified.

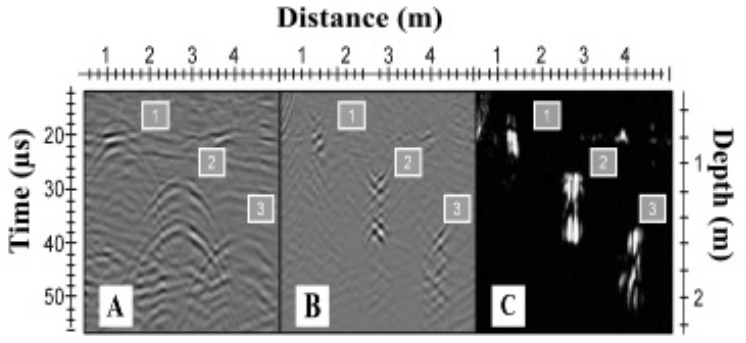

FIG. 10. Post-processing sequence of a single radargram obtained with the 500 MHz Antenna. **A**. Radargram processed with a static correction, a displacement correction, noise reduction in one and two dimensions, and gain typical adjustment. **B.** The same radargram with the Kirchhoff migration applied. The hyperbolic reflections are concentrated towards their apices. **C.** The same radargram with the Hilbert transformation applied. The magnitude of the different reflections can be compared.

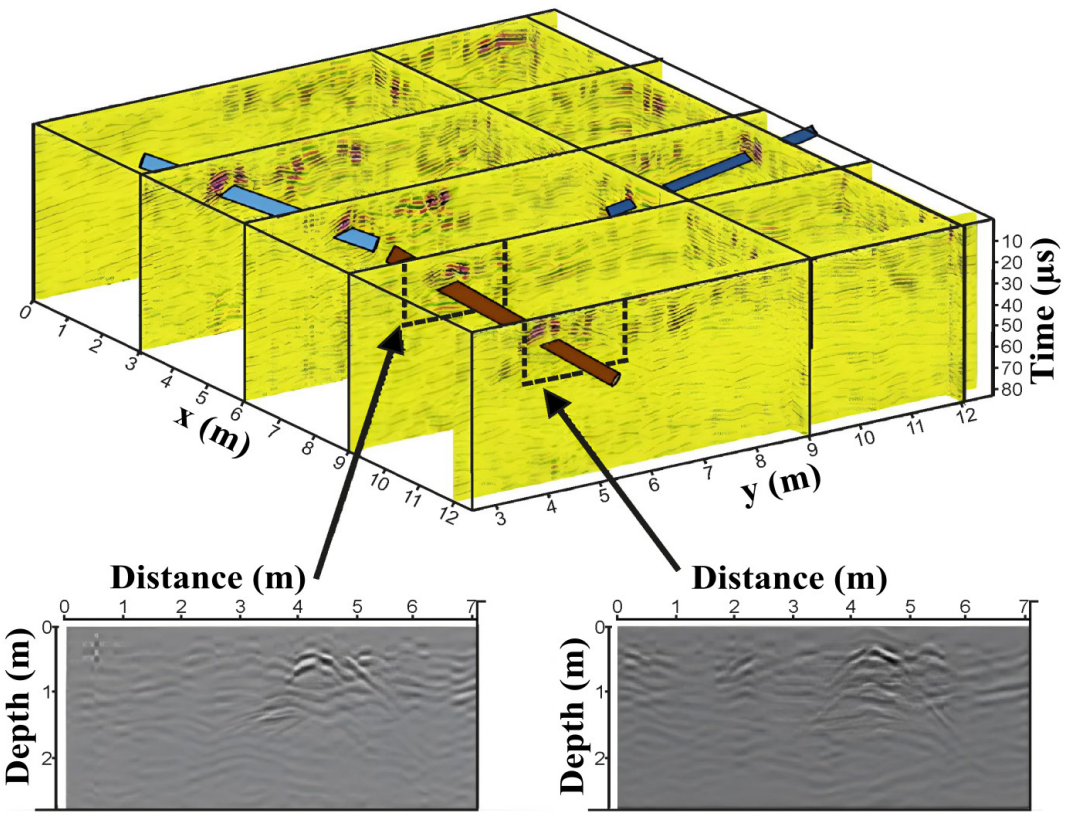

FIG. 11. 3D model of the subsoil for the north grid (3 m spacing between surveys). The sequences show common singularities detailed below in the radargrams. In a 3D modeling, local constraints are necessary to link profiles, as the one observed at 9 m in the y-axis.

the exact position of the LW (*i.e.*, orientation and depth) can be constrained by applying the Hilbert transform. In fact, the diameters of the post-processed hyperbolas in the radargrams correspond to the actual size of the logs.

7. Discussion

Ground Penetrating Radar (GPR) has been extensively employed for the detection of buried objects, ranging from archaeological investigations (Kwan and Lai, 2024) to the identification of diverse subsurface materials such as sand, timber, and concrete (Wu *et al.*, 2020), as well as for the characterization of volcanic deposits (Gertisser *et al.*, 2012). To date, however, it has not been applied to identify and characterize the stratigraphic signatures of buried large wood (LW) within volcanic deposits. Previous research has demonstrated the potential of GPR for detecting wood-related features, including the assessment of wooden structures (Pollastrelli Rodrigues *et al.*, 2021), the detection of internal defects in timber production (Halabe *et al.*, 2009), and the identification of root systems and estimation of tree biomass (Butnor *et al.*, 2016; Liu *et al.*, 2018; Lorenzo *et al.*, 2020). Furthermore, Kramer *et al.* (2012) applied this technique to investigate beaver dam structures, highlighting its effectiveness in complex environmental settings. The present study is thus a step forward in the application of GPR techniques in the knowledge related to the recruitment of logs via exhumation, moving through a more complete definition and computation of the LW budget while also addressing some of its limitations (Martin and Benda, 2001; Wohl, 2017).

The main advantages of the GPR technique are the rapidness, safeness, adequate precision, and low cost of the surveys when compared with more direct and invasive strategies, such as boreholes and trenches, which are typically expensive, time consuming, and sometimes difficult to apply in some complex environments. The main restrictions of GPR are related to the penetration capacity, since the signal can be strongly affected by the characteristics (type and grain size) of the deposits, humidity content and the dielectric parameters. In preliminary exploration initiatives, it is typically mandatory to obtain relevant information of the deposits in terms of salt and water content, the nature of the soil, and other related issues by means of geological, geotechnical, hydrogeological, and chemical antecedents. In this sense, the success of the field surveys depends not only on the adequate selection of the antennas, penetration/resolution proofs, and calibration of the acquisition parameters, but also on the informed knowledge of the local context. However, in this study, considering the prospected depths and the antennas used, the GPR technique was well fitted with the aims of the research, so the results obtained here can be extrapolated to other volcanic environments. The use of low frequency antennas can reach deeper layers and detect contrasts indicative of potential stratigraphic changes, but a higher resolution is mandatory to identify buried LW, which requires the use of high frequency antennas that have less penetration capacity. This means that for multi-purpose targets, the combination of antennas with different frequencies is a requirement.

Main errors in GPR surveys arise from the so-called false-positive results, that is, the recognition of elements which are different than those under investigation. Identifying the signature of the target elements to be explored can be a sensible first step to reduce some of these detection errors. In this sense, the use of spectral analysis by means of the Fourier transform, Wavelet analysis or comparable spectral identification techniques of the reflected waves can be of use to differentiate materials according to the frequency content of the reflections associated. In addition, a frequency domain analysis of the GPR signals can also be a valid strategy to discriminate among different elements, where a previous calibration in terms of propagation of the signal into the deposit and the subsequent reflection of the specific elements under exploration is needed. In the present case study, the conditions were ideal as the deposits are very homogenous in terms of humidity content and sediment characteristics, implying a constant dielectric parameter, aspects that made it possible to investigate the stratigraphy and its singularities, including the signature of buried wood pieces. In other volcanic environments, however, this identification could not be as straightforward because of the nature of the deposits and the potential presence of singularities embedded in the soil with similar signatures. This is the case of the Calbuco volcano, ~250 km north of Chaitén, in which similar surveys were conducted, employing comparable antennas and post-processing techniques (Barrientos, 2020), but obtaining unsatisfactory results when compared to those presented here. This comparison demonstrates that nature and conditions of the soil play a fundamental role in the selection of the geophysical technique to apply.

Considering deposit characterization, the application of bidimensional analysis with ordinary post processing techniques can be more than satisfactory to analyze the stratigraphy; however, the identification of buried wood requires more advanced post-processing techniques, for instance those based on the Kirchhoff migration and Hilbert transform. On the other hand, to analyze the spatial distribution and the length of specific buried wood elements, a 3D representation of the deposits was required, as done by Gertisser *et al*. (2012) when characterizing block and ash flow deposits generated by the Merapi volcano eruption. In our case, it was necessary to be very regular in terms of the precision of the grids, the selection of the antennas, and the location of the control points and radargrams to link the parallel surveys. A 2-3 m spacing between parallel surveys seems to be adequate for log identification purposes and a basic, first-order identification of the spatial variability of LW. To improve the level of detail of the 3D representation, it appears clear that a denser (*e.g*., 1x1 m) grid is required. The specific grid resolution, however, must be selected considering the dimensions of the LW lying on the surface. Also, the profile spacing is a local parameter that necessarily needs to be fit in the field.

The integration of complementary geophysical techniques can enhance both the stratigraphic characterization and the detection of buried elements. In this regard, geoelectrical surveys (*e.g*., electrical resistivity tomography) may be particularly useful in cases where subsurface conductivity limits the effectiveness of GPR (Knödel *et al.*, 2007). Additionally, seismic methods such as the Refraction Microtremor (ReMi) technique (Louie, 2001) can provide valuable information on deeper stratigraphic variations that are otherwise difficult to resolve using GPR or electrical resistivity tomography alone.

8. Conclusions

This study showed the applicability of the use of Ground Penetrating Radar (GPR) as a fast, low-cost, and non-invasive geophysical method to study the internal structure of the post-eruptive deposits in the Chaitén area, to detect the presence of buried large wood (LW). The main conclusions of the study are:

1. The adequate selection of the antennas, soil velocities, penetration proofs and related acquisition parameters are previous tasks that define the success of the mission. The use of multiple antennas in combination permits multiple targets. High frequency antennas (400-700 MHz) are adequate for shallow buried LW identification, whilst low frequency antennas (100-250 MHz) are more adequate for stratigraphy inspection or deeper identification of LW with important dimensions.
2. Another *in situ* previous task is the identification of the LW signature and of the reflections associated with the contrast between rock and soil. The LW signature normally depends on the nature, singularities, and humidity of the media, all of which affect the dielectric constant and the reflections associated. For this reason, the definition of control areas in which it is possible to obtain these basic parameters is desirable and required.
3. The location of buried LW and the stratigraphic characterization of the deposits studied are possible by means of a 2D analysis of the radargrams. Even though with the classical post-processing techniques, the singularities associated with LW or the linear reflections representative of stratigraphic changes can be identified; the use of more advanced post-processing strategies, such as the Kirchhoff migration and/or the Hilbert transform are more adequate to identify LW.
4. The 3D modelling of the subsoil is required to identify the spatial variability of buried LW. A well-defined grid with continuous spacing and orthogonal control surveys acting as constraints are recommended. The spacing of the profiles is key to obtaining more precise results, with a 3 m spacing or less recommended here.

The research was focused on a typical volcano-sedimentary environment in southern Chile, so the main findings can be extrapolated to similar environments elsewhere. In addition, the methodology presented here aims to facilitate the exploration of its applicability to other fluvial settings characterized by different sediment configurations and river dynamics, not limited to volcanic environments.

Acknowledgments

Authors of this work thank Agencia Nacional de Investigacion y Desarrollo (ANID, Chile) for their support through projects ANID/FONDECYT regular 1141064 and 1200079. In addition, authors acknowledge Natural and Anthropogenic Risks Research Center (RiNA) at Universidad Austral de Chile. M. San Juan and two anonymous reviewers helped revising this manuscript.

References

Ashworth, P.J.; Sambrook Smith, G.H.; Best, J.L.; Bridge, J.S.; Lane, S.N.; Lunt, I.A.; Reesink, A.J.H.; Simpson, C.J.; Thomas, R.E. 2011. Evolution and sedimentology of a channel fill in the sandy braided South Saskatchewan River and its comparison to the deposits of an adjacent compound bar. Sedimentology 58 (7): 1860-1883. https://doi.org/10.1111/j.1365-3091.2011.01242.x

Baker, G.; Jordan, T.; Pardy, J. 2007. An introduction to ground penetrating radar (GPR). *In* Stratigraphic Analyses Using GPR (Baker. G.S.; Jol, H.M.; editors). The Geological Society of America 432: 1-18. Boulder. https://doi.org/10.1130/2007.2432(01)

Barrientos, J. 2020. Aplicación de métodos geofísicos para la caracterización de la estructura de los depósitos del Río Blanco Este, Volcán Calbuco, Región de Los Lagos, Chile. MSc Thesis (Unpublished), Universidad Austral de Chile: 243 p.

Benda, L.; Bigelow, P. 2014. On the patterns and processes of wood in northern California streams. Geomorphology 209: 79-97. https://doi.org/10.1016/j.geomorph.2013.11.028

Boivin, M.; Buffin-Bélanger, T.; Piégay, H. 2017. Estimation of large wood budgets in a watershed and river corridor at interdecadal to interannual scales in a cold temperate fluvial system. Earth Surface Processes and Landforms 42: 2199-2213. https://doi.org/10.1002/esp.4174

Borden, K.A.; Isaac, M.E.; Thevathasan, N.V.; Gordon, A.M.; Thomas, S.C. 2014. Estimating coarse root biomass with ground penetrating radar in a tree-based intercropping system. Agroforestry Systems 88 (4): 657-669. https://doi.org/10.1007/s10457-014-9722-5

Burke, M.J.; Woodward, J.; Russell, A.J.; Fleisher, P.J.; Bailey, P.K. 2008. Controls on the sedimentary architecture of a single event englacial esker: Skeidararjökull, Iceland. Quaternary Science Reviews 27: 1829-1847. https://doi.org/10.1016/j.quascirev.2008.06.012

Burke, M.J.; Woodward, J.; Russell, A.J. 2010. Sedimentary architecture of large-scale, jökulhlaup-generated, ice-block obstacle marks: Examples from Skeidararjökull, SE Iceland. Sedimentary Geology 227 (1-4): 1-10. https://doi.org/10.1016/j.sedgeo.2010.03.001

Butnor, J.R.; Doolittle, J.A.; Kress, L.; Cohen, S.; Johnsen, K.H. 2001. Use of ground-penetrating radar to study tree roots in the southeastern United States. Tree Physiology 21 (17): 1269-1278. https://doi.org/10.1093/treephys/21.17.1269

Butnor, J.R.; Samuelson, L.J.; Stokes, T.A.; Johnsen, K.H.; Anderson, P. H.; González-Benecke, C. A. 2016. Surface-based GPR underestimates below-stump root biomass. Plant and Soil 402 (1-2): 47-62. https://doi.org/10.1007/s11104-015-2768-y

Cassidy, N.J.; Russell, A.J.; Marren, P.M.; Fay, H.; Knudsen, O.; Rushmer, E.L.; Van Dijk, T.A.G.P. 2003. GPR derived architecture of November 1996 jökulhlaup deposits, Skeidarársandur, Iceland. *In* Ground Penetrating Radar in Sediments: Applications and Interpretation (Bristow, C.S.; Jol, H.M.; editors). Geological Society of London, Special Publication 211: 153-166. London. https://doi.org/10.1144/GSL.SP.2001.211.01.13

Foster, D.R.; Knight, D.H.; Franklin, J.F. 1998. Landscape patterns and legacies resulting from large infrequent forest disturbances. Ecosystems 1:.497-510.

Fuentes, C.F. 2016. Uso de radar de penetración terrestre (GPR) para caracterización de depósitos de sedimento volcánico y madera muerta enterrada: aplicación a la cuenca del río Blanco, Chaitén, Chile. Thesis dissertation (unpublished), Universidad Austral de Chile: 10 p.

Gertisser, R.; Cassidy, N.J.; Charbonnier, S.J.; Nuzzo, L.; Preece, K. 2012. Overbank block-and-ash flow deposits and the impact of valley-derived, unconfined flows on populated areas at Merapi volcano, Java, Indonesia. Natural Hazards 60 (2): 623-648. https://doi.org/10.1007/s11069-011-0044-x

Gomez, C.; Lavigne, F.; Lespinasse, N.; Hadmoko, D.S.; Wassmer, P. 2008. Longitudinal structure of pyroclastic-flow deposits, revealed by GPR survey, at Merapi Volcano, Java, Indonesia. Journal of Volcanology and Geothermal Research 176 (4): 439-447. https://doi.org/10.1016/j.jvolgeores.2008.04.012

Guo, L.; Chen, J.; Cui, X.; Fan, B.; Lin, H. 2013. Application of ground penetrating radar for coarse root detection and quantification: a review. Plant and Soil 362 (1-2): 1-23. https://doi.org/10.1007/s11104-012-1455-5

Halabe, U.B.; Agrawal, S.; Gopalakrishnan, B. 2009. Nondestructive evaluation of wooden logs using ground penetrating radar. Nondestructive Testing and Evaluation 24 (4): 329-346. https://doi.org/10.1080/10589750802474344

Hornung, J.; Pflanz, D.; Hechler, A.; Beer, A.; Hinderer, M.; Maisch, M.; Bieg, U. 2010. 3-D architecture, depositional patterns and climate triggered sediment fluxes of an alpine alluvial fan (Samedan, Switzerland). Geomorphology 115 (3-4): 202-214. https://doi.org/10.1016/j.geomorph.2009.09.001

Iroumé, A.; Mao, L.; Andreoli, A.; Ulloa, H.; Ardiles, M.P. 2015. Large wood mobility processes in low-order

Chilean river channels. Geomorphology 228: 681-693. https://doi.org/10.1016/j.geomorph.2014.10.025

Iroumé, A.; Ruiz-Villanueva, V.; Picco, L. 2017. Breakdown of instream wood in low order forested streams of the Southern Chilean mountain ranges. Forest Ecology and Management 401: 17-32. https://doi.org/10.1016/j.foreco.2017.06.058

Iroumé, A.; Cartagena, M.; Villablanca, L.; Sanhueza, D.; Mazzorana, B.; Picco, L. 2020a. Long-term large wood load fluctuations in two low order streams in southern Chile. Earth Surface Processes and Landforms 45 (9): 1959-1973. https://doi.org/10.1002/esp.4858

Iroumé, A.; Paredes, A.; Garbarino, M.; Morresi, D.; Batalla, R.J. 2020b. Post-eruption morphological evolution and vegetation dynamics of the Blanco River, southern Chile. Journal of South American Earth Sciences 104. https://doi.org/10.1016/j.jsames.2020.102809

Jara, C. 2015. Exploración geofísica mediante la técnica del Radar de Penetración Terrestre: un estado del conocimiento. Thesis dissertation (Unpublished), Universidad Austral de Chile: 139 p. Chile.

Jinder, J.; Chang, S.; Yu, H. 2006. GPR reflection characteristics and depositional models of mud volcanic sediments-Wushanting mud volcano field, southwestern Taiwan. Journal of Applied Geophysics 60 (3-4): 179-200. https://doi.org/10.1016/j.jappgeo.2006.03.001

Knödel, K.; Lange, G.; Voigt, H.J. 2007. Environmental geology: handbook of field methods and case studies. Springer-Verlag: 547 p. Hannover.

Kramer, N.; Wohl, E.E.; Harry, D.L. 2012. Using ground penetrating radar to 'unearth' buried beaver dams. Geology 40 (1): 43-46. https://doi.org/10.1130/G32682.1

Kwan, Y. R.L.; Lai, W. 2024. Archaeological investigation of burials preluded by ground penetrating radar and geospatial technologies. Journal of Archeological Science 170. https://doi.org/10.1016/j.jas.2024.106058

Liu, X.; Dong, X.; Xue, Q.; Leskovar, D.I.; Jifon, J.; Butnor, J.R.; Marek, T. 2018. Ground penetrating radar (GPR) detects fine roots of agricultural crops in the field. Plant and Soil 423 (1-2): 517-531. https://doi.org/10.1007/s11104-017-3531-3

Lorenzo, H.; Pérez-Gracia, V.; Novo, A.; Armesto, J. 2020. Forestry applications of ground-penetrating radar. Forest Systems 19 (1): 5-17. https://doi.org/10.5424/fs/2010191-01163

Louie, J. 2001. Faster, better: Shear-Wave velocity to 100 meters depth from refraction microtremor arrays. Bulletin of the Seismological Society of America 91: 347-364. https://doi.org/10.1785/0120000098

Major, J.J.; Lara, L.E. 2013. Overview of Chaitén Volcano, Chile, and its 2008-2009 eruption. Andean Geology 40 (2): 196-215. doi: http://dx.doi.org/10.5027/andgeoV40n2-a01

Major, J.J.; Pierson, T.C.; Hoblitt, R.P.; Moreno, H. 2013. Pyroclastic density currents associated with the 2008-09 eruption of Chaitén volcano (Chile): forest disturbances, deposits, and dynamics. Andean Geology 40 (2): 324-358. http://dx.doi.org/10.5027/andgeoV40n2-a09

Major, J.J.; Bertin, D.; Pierson, T.C.; Amigo, Á.; Iroumé, A.; Ulloa, H.; Castro, J. 2016. Extraordinary sediment delivery and rapid geomorphic response following the 2008-2009 eruption of Chaitén Volcano, Chile. Water Resources Research 52 (7): 5075-5094. https://doi.org/10.1002/2015WR018250

Martin, D.J.; Benda, L.E. 2001. Patterns of Instream Wood Recruitment and Transport at the Watershed scale. Transactions of the American Fisheries Society 130 (5): 940-958. https://doi.org/10.1577/1548-8659(2001)130<0940:POIWRA>2.0.CO;2

Martini, L.; Picco, L.; Iroumé, A.; Cavalli, M. 2019. Sediment connectivity changes in an Andean catchment affected by volcanic eruption. Science of the Total Environment 692: 1209-222. https://doi.org/10.1016/j.scitotenv.2019.07.303

May, C.L.; Gresswell, R.E. 2003. Processes and Rates of Sediment and Wood Accumulation in Headwater streams of the Oregon Coast Range, USA. Earth Surface Processes and Landforms 28 (4): 409-424.

Neto, P.X.; De Medeiros, W.E. 2006. A practical approach to correct attenuation effects in GPR data. Journal of Applied Geophysics 59 (2): 140-151. https://doi.org/10.1016/j.jappgeo.2005.09.002

Oppenheim, A.V.; Schafer, R.W. 2014. Discrete-time signal processing (3rd edit). Prentice-Hall Signal Processing Series: 1120 p. USA.

Özdemir, C.; Demirci, Ş.; Yiğit, E.; Yilmaz, B. 2014. A review on migration methods in b-scan ground penetrating radar imaging. Mathematical Problems in Engineering. https://doi.org/10.1155/2014/280738

Picco, L.; Tonon, A.; Rainato, R.; Lenzi, M.A. 2016. Bank erosion and large wood recruitment along a gravel bed river. Journal of Agricultural Engineering 47 (2): 72-81. https://doi.org/10.4081/jae.2016.488

Picco, L.; Scalari, C.; Iroumé, A.; Mazzorana, B.; Andreoli, A. 2021. Large wood load fluctuations in an Andean basin. Earth Surface Processes and Landforms 46 (2): 371-384. https://doi.org/10.1002/esp.5030

Pierson, T.; Major, J. 2014. Hydrogeomorphic effects of explosive volcanic eruptions on drainage basins. Annual Review of Earth and Planetary Sciences 42: 469-507. https://doi.org/10.1146/annurev-earth-060313-054913

Pierson, T.; Major, J.; Amigo, A.; Moreno, H. 2013. Acute sedimentation response to rainfall following the explosive phase of the 2008-09 eruption of Chaitén volcano, Chile. Bulletin of Volcanology 75 (5): 1-17. https://doi.org/10.1007/s00445-013-0723-4

Pollastrelli Rodrigues, B.; Senalik, C.A.; Wu, X.; Wacker, J. 2021. Use of Ground Penetrating Radar in the Evaluation of Wood Structures: A Review. Forests 12 (4): https://doi.org/10.3390/f12040492

Pujari, P.R.; Pardhi, P.; Muduli, P.; Harkare, P.; Nanoti, M.V. 2007. Assessment of pollution near landfill site in Nagpur, India by resistivity imaging and GPR. Environmental Monitoring and Assessment 131 (1-3): 489-500. https://doi.org/10.1007/s10661-006-9494-0

Reeves, G.H.; Burnett, K.M.; McGarry, E.V. 2003. Sources of large wood in the main stream of a fourth-order watershed in coastal Oregon. Canadian Journal of Forest Research 33: 1363-1370. https://doi.org/10.1139/x03-095

Rey, J.; Martínez, J.; Hidalgo, M.C. 2013. Investigating fluvial features with electrical resistivity imaging and ground-penetrating radar: The Guadalquivir River terrace (Jaen, Southern Spain). Sedimentary Geology 295: 27-37. https://doi.org/10.1016/j.sedgeo.2013.07.003

Sandmeier, K.J. 2009. ReflexW, User`s Manual. Sandmeier Geophysical Research 728 p. Germany.

Satriani, A.; Loperte, A.; Proto, M.; Bavusi, M. 2010. Building damage caused by tree roots: laboratory experiments of GPR and ERT surveys. Advances in Geosciences 24 (24): 133-137. https://doi.org/10.5194/adgeo-24-133-2010

Schenk, E.R.; Moulin, B.; Hupp, C.R.; Richter, J.M. 2014. Large wood budget and transport dynamics on a large river using radio telemetry. Earth Surface Processes and Landforms 39 (4): 487-498. https://doi.org/10.1002/esp.3463

Swanson, F.J.; Jones, J.A.; Crisafulli, C.M.; Lara, A. 2013. Effects of volcanic and hydrologic processes on forest vegetation: Chaitén Volcano, Chile. Andean Geology 40 (2): 359-391. http://dx.doi.org/10.5027/andgeoV40n2-a10

Tonon, A.; Iroumé, A.; Picco, L.; Oss-Cazzador, D.; Lenzi, M.A. 2017. Temporal variations of large wood abundance and mobility in the Blanco River affected by the Chaitén volcanic eruption, southern Chile. Catena 156: 149-160. https://doi.org/10.1016/j.catena.2017.03.025

Tonon, A.; Picco, L.; Rainato, R. 2018. Test of methodology for developing a large wood budget: A 1-year example from a regulated gravel bed river following ordinary floods. Catena 165: 115-124. https://doi.org/10.1016/j.catena.2018.01.035

Ulloa, H.; Iroumé, A.; Mao, L.; Andreoli, A.; Diez, S.; Lara, L.E. 2015. Use of remote imagery to analyze changes in morphology and longitudinal large wood distribution in the Blanco River after the 2008 Chaitén volcanic eruption, southern Chile. Geografiska annaler. Series A, Physical geography 97 (3): 523-541. https://doi.org/10.1111/geoa.12091

Utsi, E. 2014. Target resolution using very high frequency Ground Penetrating Radar. *In* Structural Faults and Repair (Forde, M.; editor). Proceedings Conference, July 2014, Imperial College. London.

Wohl, E. 2013. Floodplains and wood. Earth-Science Reviews 123: 194-212. https://doi.org/10.1111/geoa.12091

Wohl, E. 2017. Bridging the gaps: an overview of wood across time and space in diverse rivers. Geomorphology 279: 3-26. https://doi.org/10.1016/j.geomorph.2016.04.014

Wu, X.; Senalik, C.A.; Wacker, J.; Wang, X.; Li, G. 2020. Object Detection of Ground-Penetrating Radar Signals Using Empirical Mode Decomposition and Dynamic Time Warping. Forests 11 (2). https://doi.org/10.3390/f11020230

Yelf, R.; Yelf, D. 2004. Where is true time zero? Electromagnetic Phenomena 7: 279-282.

Manuscript received: July 17, 2024; revised/accepted: November 21, 2025; available online: December 11, 2025.